



## Pulsed Galvanostatic Deposition of Pt Particles on Microcrystalline and Nanocrystalline Diamond Thin-Film Electrodes

### I. Characterization of As-Deposited Metal/Diamond Surfaces

Jason A. Bennett,\* Yoshiyuki Show, Shihua Wang, and Greg M. Swain\*\*<sup>z</sup>

Department of Chemistry, Michigan State University, East Lansing, Michigan 48824-1322, USA

The pulsed galvanostatic deposition of nanometer-sized Pt particles on electrically conducting microcrystalline and nanocrystalline diamond thin-film electrodes is reported. The deposition was studied as a function of pulse number (10-50) and current density (0.50-1.50 mA cm<sup>-2</sup>) at the two morphologically different forms of diamond. The deposition of catalyst particles using ten 1 s pulses (duty cycle 50%) at a current density of 1.25 mA cm<sup>-2</sup> (geometric area) produced the smallest nominal particle size and the highest particle coverage on both diamond surfaces. Secondary electron micrographs revealed metal particle deposition over much of the diamond surface, a nominal particle size of 43 ± 27 nm [relative standard deviation (RSD) = 63%] for microcrystalline and 25 ± 25 nm (RSD = 100%) for nanocrystalline diamond, and a nominal particle coverage of 7.5 (±0.9) × 10<sup>9</sup> cm<sup>-2</sup> for microcrystalline and 1.9 (±1.0) × 10<sup>10</sup> cm<sup>-2</sup> for nanocrystalline diamond. Deposition under these conditions resulted in the most efficient utilization of the metal catalyst for H<sup>+</sup> adsorption, based on the electrochemically active Pt area normalized to the estimated metal loading. Typical specific surface areas of 10-50 m<sup>2</sup>/g Pt were calculated, which compare favorably to values obtained at sp<sup>2</sup> electrodes, like carbon and graphite. The influence of the diamond electrode microstructural and electronic properties on the formation of dimensionally uniform metal adlayers is discussed.

© 2005 The Electrochemical Society. [DOI: 10.1149/1.1890745] All rights reserved.

Manuscript submitted May 31, 2004; revised manuscript received October 1, 2004. Available electronically April 11, 2005.

Carbon-supported metal catalysts are widely used in electrochemical technologies. For example, dispersed Pt particles on high-surface-area carbon supports are used as catalysts for hydrogenation and oxidation reactions, such as for both hydrogen oxidation and oxygen reduction in phosphoric acid (PAFCs) and proton exchange membrane fuel cells (PEMFCs).<sup>1,2</sup> Platinum is the best electrocatalyst for the oxygen reduction reaction (ORR), an important reaction in biological systems and fuel cells.<sup>3-13</sup> Among the carbon support materials regularly employed, activated carbons are probably the most common. Activated carbons possess a turbostratic microstructure of sp<sup>2</sup>-bonded carbon with a high surface area and microporosity.<sup>1,2</sup> The properties of the electrocatalyst support material are crucial for the operational performance.<sup>1-3,14,15</sup> The primary role of the support is to provide a high surface area over which highly dispersed, nanometer-sized electrocatalyst particles can be dispersed and stabilized. Highly dispersed supported catalysts are attractive for electrochemical processes because a high electrochemically active surface area can be achieved with a low loading of the normally expensive electrocatalyst.

As mentioned previously, current electrocatalyst support materials are generally porous, sp<sup>2</sup>-bonded carbon materials (*e.g.*, physically or chemically activated carbon or carbon black). These materials function well in many applications but are susceptible to oxidation and/or corrosion in the presence of reactive oxygen, in aggressive chemical environments and/or under harsh electrochemical conditions.<sup>1,2,15,16</sup> The oxidation/corrosion causes morphological and microstructural damage that leads to decreased catalytic activity due to catalyst detachment, aggregation, and/or fouling by gasification products. Complete electrode failure can result if the degradation is severe enough.

Advanced electrocatalyst support materials are needed for those demanding applications where conventional sp<sup>2</sup>-bonded carbon supports fail. One example of this occurs in fuel cells during start-up and shut-down as a local cathode potential as high as 1.5 V can be reached, which is a potential well positive of the thermodynamic value.<sup>17</sup> Carbon corrosion can occur at such high voltages and this leads to degradation of the stack voltage. Our group has been investigating the use of electrically conducting polycrystalline diamond

as an advanced carbon electrocatalyst support material.<sup>18-21</sup> There are two technical challenges in this endeavor: development of electrically conducting diamond (*e.g.*, powder) with high surface area and establishment of a protocol for depositing and stabilizing highly dispersed electrocatalyst particles on the diamond support. Thus far, our efforts have been focused on the latter task with the goals of (*i*) determining the dimensional stability of diamond thin film (low surface area) under a variety of electrochemical conditions<sup>19</sup> and (*ii*) studying the formation of electrocatalytic Pt adlayers on the film surface.<sup>20</sup> Diamonds possess properties that make it an attractive support material: dimensional stability, resistance to corrosion, and the ability to operate for extended periods of time in harsh chemical environments at high potential, current density, and temperature without microstructural or morphological degradation.<sup>21,22</sup>

Two types of electrically conducting diamond thin film are under investigation: microcrystalline (>1 μm crystallite size) and nanocrystalline (~10 to 20 nm crystallite size).<sup>23-28</sup> Each possesses a different morphology and microstructure, but both exhibit similar electrical conductivity and electrochemical activity when highly doped with boron. The formation of metal phases on polycrystalline diamond has been reported.<sup>20,29-33</sup> A common observation, though, is weak attachment of the metal particles to the hydrogen-terminated diamond surface.<sup>19,20,31,32</sup> Consequently, the metal particles are easily dislodged from the surface by gas evolution, for instance. In an effort to better stabilize the metal particles, we have adopted an approach whereby a short secondary diamond growth is applied to the metal-coated surface. This secondary growth entraps the metal particles into the surface microstructure without causing major loss in the electrocatalytic activity. We refer to these as metal/diamond composite electrodes.<sup>19-21</sup> This sequential diamond growth/Pt deposition/secondary diamond growth procedure produces a dimensionally stable and electrically conductive catalytic electrode. The metal catalyst particles are strongly anchored in the microstructure by the secondary diamond growth. For instance, no morphological or microstructural damage and no lost catalyst activity were observed after two 1 h periods of anodic polarization in 85% H<sub>3</sub>PO<sub>4</sub> at 170°C and 0.1 A cm<sup>-2</sup>.<sup>19</sup> In comparison, a Pt-impregnated sp<sup>2</sup> carbon cloth electrode (E-Tek) failed catastrophically within the first few minutes of exposure to the same conditions.

We have previously studied the formation of Pt adlayers on diamond by dc magnetron sputtering<sup>18</sup> and electrodeposition, both constant potential and current.<sup>19,20</sup> Electrodeposition is the preferred method of the two because it affords better control over the particle

\* Electrochemical Society Student Member.

\*\* Electrochemical Society Active Member.

<sup>z</sup> E-mail: swain@chemistry.msu.edu

size and coverage. Despite the excellent dimensional stability of the Pt/diamond composite electrode, the nominal Pt particle size produced was too large and the coverage too low to be practical. For example, the particle size varied from 50 to 300 nm and the particle coverage was in the  $10^8 \text{ cm}^{-2}$  range for metal phase formation at constant current.<sup>19,20</sup> Low loadings of highly dispersed metal particles are desired for a practical supported catalyst. Pulsed galvanostatic deposition can produce metal particles that are nominally smaller in size and more uniformly distributed over a surface compared to what is achieved using constant current deposition. Pulsed electrodeposition approaches have been employed to prepare nanometer-sized particles of metals and alloys.<sup>33-45</sup> Individual particle growth is favored as the conditions are selected to minimize overlap of reactant depletion layers from neighboring particles. Maintaining separate depletion layers around each particle results in similar growth rates for all and leads to more highly dispersed particles of nominally smaller size.

We report herein on the use of pulsed galvanostatic deposition to form Pt adlayers on both microcrystalline (BMD) and nanocrystalline (BND) diamond thin films. This work is a continuation of our effort to control and understand metal phase formation on diamond. The purpose for the work was to learn how the nucleation and growth of Pt electrocatalyst particles on both diamond types is affected by the pulse current density and pulse number. In particular, the spatial distribution of the deposits over the surface, the nominal particle size and variance, and the particle coverage were the factors of interest. Another objective was to learn how the diamond film morphology and microstructure affect the metal phase formation. Polycrystalline diamond is a heterogeneous electrode material in terms of its microstructural and electronic properties, which complicates the study of metal phase formation. The microstructural and electronic properties certainly play a key role in the kinetics of metal electrodeposition and the time-dependent surface morphology of the deposits. The uncoated and coated diamond electrodes were characterized by scanning electron microscopy (SEM), cyclic voltammetry, and conductivity-probe atomic force microscopy (CP-AFM).

## Experimental

**Diamond thin-film deposition.**—Microcrystalline and nanocrystalline diamond thin-film electrodes were deposited using microwave-assisted plasma chemical vapor deposition (CVD; 1.5 kW, 2.54 GHz, Astex, Inc., Lowell, MA) on highly conducting p-Si(100) substrates ( $<0.001 \Omega \text{ cm}$ , Virginia Semiconductor, Inc.). The substrates were pretreated by mechanical polishing on a felt pad for 5 min using a 2  $\mu\text{m}$  diam diamond powder (GE Super-abrasives, Worthington, OH) slurred with ultrapure water (18 M $\Omega$ ). After polishing, the substrates were rinsed with ultrapure water and 2-propanol. The substrates were then ultrasonically cleaned in acetone, 2-propanol, and ultrapure water (5 min each). The microcrystalline films were deposited for 10 h using a methane-to-hydrogen ( $\text{CH}_4/\text{H}_2$ ) source gas ratio of 0.50%. The total gas flow was 200 sccm with the microwave power, pressure, and temperature held constant at 1 kW, 45 Torr, and  $\sim 800^\circ\text{C}$ , respectively. The nanocrystalline films were deposited using gas flow rates of 1, 94, and 5 sccm for  $\text{CH}_4$ , Ar, and  $\text{H}_2$ , respectively. These films were grown for *ca.* 2 h using a microwave power of 800 W, a deposition pressure of 140 Torr, and a temperature of  $\sim 800^\circ\text{C}$ . All gases were ultrahigh purity (99.999%) grade ( $\text{CH}_4$  and  $\text{H}_2$  from AGA Specialty Gas, Cleveland, OH, and Ar from BOC Group, Inc., Murray Hill, NJ). The film thickness was 3-7  $\mu\text{m}$  for both film types.

Both film types were doped from the gas phase by adding 10 ppm  $\text{B}_2\text{H}_6$  [2.0 (microcrystalline) and 1.0 (nanocrystalline) sccm, respectively, of 0.1%  $\text{B}_2\text{H}_6$  diluted in  $\text{H}_2$ , Matheson Gas Products, Inc.] to the source gas mixture. Following the deposition, the  $\text{CH}_4$  and  $\text{B}_2\text{H}_6$  flows were stopped, and the films remained exposed to the  $\text{H}_2$  (BMD) or  $\text{H}_2/\text{Ar}$  (BND) plasma for an additional 10 min.

They were then gradually cooled over several minutes to less than  $400^\circ\text{C}$  in the presence of atomic hydrogen by reducing the microwave power and system pressure. This postgrowth annealing in atomic hydrogen serves to etch away adventitious nondiamond carbon impurity, minimize dangling bonds, and ensure maximum hydrogen termination. Both film types had a nominal boron dopant concentration of *ca.*  $10^{20} \text{ B cm}^{-3}$  and a film resistivity of less than  $0.05 \Omega \text{ cm}$ .

**Electrochemical measurements.**—All electrochemical measurements were performed at room temperature in a single-compartment glass cell using a CH Instruments model 650A electrochemical workstation (CH Instruments, Inc., Austin, TX). The design of the electrochemical cell was reported previously.<sup>46</sup> The diamond electrodes were pressed against the bottom of a glass cell. A Viton O-ring was used to contain the solution and define the exposed electrode area,  $0.2 \text{ cm}^2$ . All currents are normalized to this area unless otherwise noted. An Ag/AgCl reference electrode was positioned in close proximity to the working electrode using a cracked-glass capillary filled with 4 M KCl. All potentials reported herein are referenced to this electrode. A large-area carbon rod served as the auxiliary electrode and was positioned normal to the working electrode. Electrical connection was made to the working electrode by contacting the back side of the cleaned Si substrate with a clean Cu plate. The clean Si surface was rubbed with a graphite rod prior to contacting the Cu plate. Once mounted in the cell, the electrode surface was cleaned by soaking in distilled 2-propanol for 20 min.<sup>47</sup> The diamond films were characterized, prior to Pt deposition, using several redox systems [ $\text{Fe}(\text{CN})_6^{3-/4-}$ ,  $\text{Ru}(\text{NH}_3)_6^{3+/2+}$ ,  $\text{Fe}^{3+/2+}$ , and  $\text{IrCl}_6^{2-/3-}$ ] to evaluate the electrode response over a wide potential range, as reported elsewhere.<sup>27,28,46</sup> All chemicals were reagent grade quality or better, and used without additional purification. The 1 mM solutions of potassium ferrocyanide (Aldrich), hexammineruthenium(III) chloride (Aldrich), and ferric sulfate (Fisher), and the 0.1 mM solution of potassium hexachloroiridate(IV) (Aldrich) were prepared fresh daily. The supporting electrolyte was either 1 M KCl (Spectrum) or 0.1 M  $\text{HClO}_4$  (redistilled, 99.999%, Aldrich). For most experiments, the solutions were first degassed by bubbling  $\text{N}_2$  for at least 10 min, and then maintained under an  $\text{N}_2$  blanket during the measurement.

After evaluating an electrode response, the cell was thoroughly rinsed with ultrapure water and filled with 1 mM potassium hexachloroplatinate(IV) (98%, Aldrich) dissolved in 0.1 M  $\text{HClO}_4$ . The solution was purged with  $\text{N}_2$  for 20 min prior to deposition. Nanometer-sized Pt particles were deposited under an  $\text{N}_2$  blanket using the pulsed galvanostatic method. The hardware consisted of a homemade galvanostat, configured from an OMNI 90 potentiostat (Cypress Systems, Inc., Lawrence, KS) that was interfaced with a PCI-6034E controller and data acquisition board (National Instruments, Austin, TX). The pulse generation was computer-controlled using National Instruments LabVIEW software (version 5.1 or 6.0). All pulses were 1 s in length with a 1 s delay time between each, which is a 50% duty cycle (pulse time/period). The pulse number and current density were systematically investigated to determine the optimum deposition conditions in terms of metal particle size and coverage.

After depositing the metal, the platinate solution was removed and the cell was carefully rinsed with ultrapure water by flowing the water down the sides of the glass cell. Metal particles generally weakly adhere to the hydrogen-terminated diamond surface, and vigorous rinsing can result in significant particle detachment. The cell was then filled with a fresh 0.1 M  $\text{HClO}_4$  solution, again by pouring the solution down the sides of the cell, and purged with  $\text{N}_2$  for 30 min. The gas was introduced far enough from the surface so as to not disturb the catalyst particles. Under the  $\text{N}_2$  blanket, the potential was cycled ten times between  $-200$  and  $1300 \text{ mV vs. Ag/AgCl}$  to clean the Pt deposits. The potential was kept within this window to avoid significant gas evolution. The voltammetric i-E curve usually stabilized within five cycles. The charge for  $\text{H}^+$  ad-

sorption was used to determine the electrochemically active Pt surface area, assuming a 1H:1Pt surface interaction and a coulombic charge of  $210 \mu\text{C}/\text{cm}^2$  for hydrogen adsorption on an atomically flat Pt(111) surface.<sup>48-50</sup>

Glassy carbon was used in some comparison measurements. The electrode (GC-30, Tokai, Ltd., Japan) was mechanically polished on separate felt polishing cloths using aqueous slurries of 1.0, 0.3, and  $0.05 \mu\text{m}$  diam deagglomerated alumina powder (Buehler, Ltd., Illinois). After each polishing step, the electrode was copiously rinsed with ultrapure water and ultrasonically cleaned in this medium for 10-15 min. After the final polishing and sonication step, the electrode was dried in a stream of  $\text{N}_2$  electrode and placed in the electrochemical cell where it was exposed to distilled isopropanol for 10 min as a final cleaning step.

**Physical characterization.**—The films were physically characterized using a JSM-6400V scanning electron microscope (JEOL, Ltd., Tokyo, Japan). Micrographs were recorded using both secondary and backscattered electrons generated with an accelerating voltage of 20 kV. The presence of Pt was verified by energy-dispersive X-ray (EDX) analysis (Noran Instruments, Inc., Middleton, WI) in conjunction with the JSM-6400V. Particle analysis was performed using the ANALYSIS imaging software (Software Imaging System Corp., Lakewood, CO).

CP-AFM measurements were carried out with a NanoScope IIIa (Veeco Instruments, CA). A Au-coated silicon tip was used in the contact mode. A homemade electrical circuit was used to measure the current flowing between the conductive tip and the electrode surface as the tip was rastered over an area. The diamond samples were placed on a metal stage and electrical contact was made to the bottom of the conducting Si substrate using carbon tape. A bias voltage was applied between the tip and the substrate, +2 V. Conductivity maps were generated simultaneously with the topographical images.

Atomic absorption spectrometry (AAS) was used to determine the catalyst loading for a given set of deposition conditions. For these measurements, the Pt particles were deposited on a separate set of diamond film as a function of the current density and pulse number. After deposition, the Pt metal was then dissolved from the electrode by soaking for 1 h in 4 mL of warm aqua-regia, which consisted of 3 mL HCl (36.5-38.0%, Columbus Chemical Industries, Inc., Columbus, WI) and 1 mL  $\text{HNO}_3$  (70%, Columbus Chemical Industries, Inc., Columbus, WI). Pt is known to dissolve in warm aqua-regia while diamond is quite stable in this solution and undergoes no morphological alteration.<sup>19,20</sup> Upon cooling to room temperature, the electrode was removed from the solution and rinsed thoroughly with ultrapure water. The rinses were collected and mixed with the original solution to collect all the dissolved metal. The total solution volume was 50 mL. AAS was performed directly on this solution using a Hitachi Z-9000 atomic absorption spectrophotometer (Hitachi, Ltd., Tokyo, Japan) with a graphite tube furnace. The metal ion concentration in each solution was determined from multiple measurements in order to estimate the metal loading.

## Results

**Pt deposition on microcrystalline diamond.**—Pt metal was deposited onto the diamond surface by pulsed galvanostatic deposition with the pulse width and current density maintained constant at 1 s and  $0.50 \text{ mA}/\text{cm}^2$  (geometric area), respectively, and a pulse number of either 10, 25, or 50. Figure 1a-c shows secondary electron micrograph (SEM) images of Pt-coated microcrystalline diamond thin-film electrodes for these three pulse numbers. EDX analysis confirmed that the bright spots are indeed Pt particles. The particles decorate both the grains and grain boundaries, indicating that most regions of the polycrystalline film are electrochemically active and support charge transfer. The formation of the multilayer islands or particles is consistent with a Volmer-Weber mechanism of

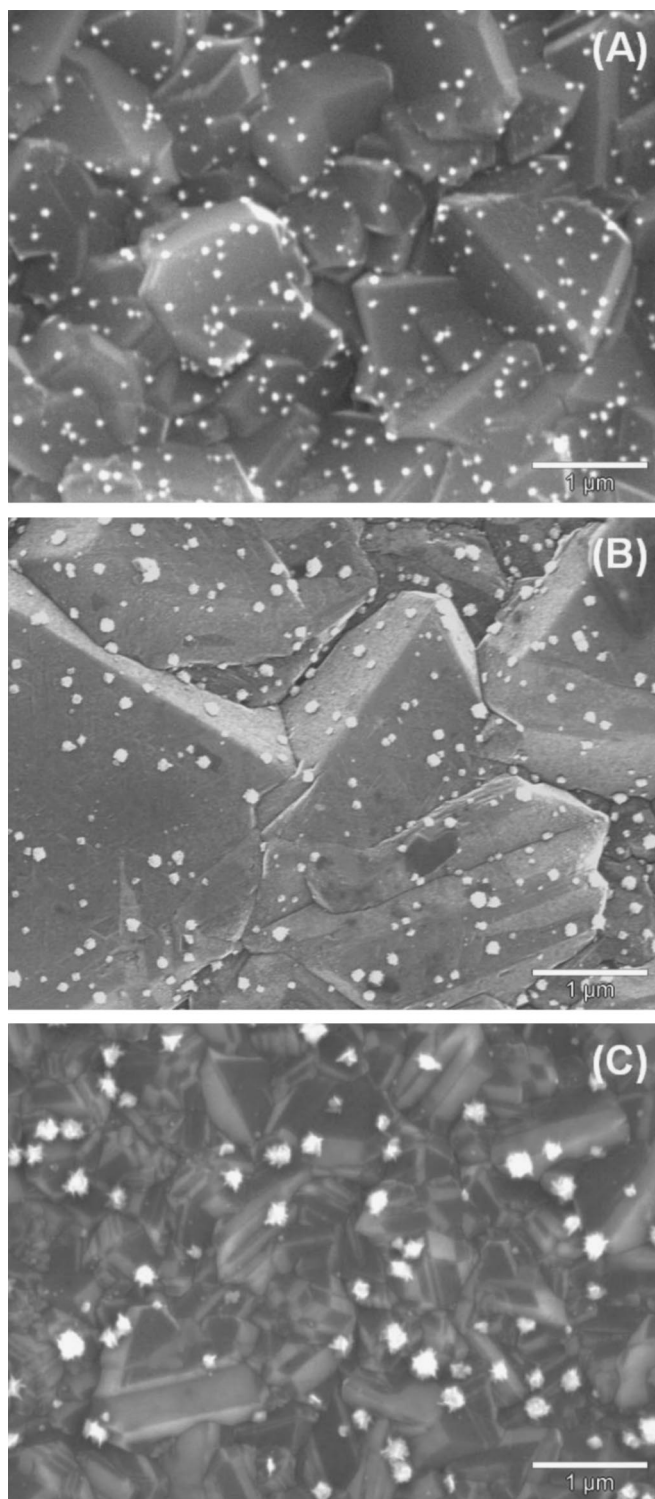


**Figure 1.** SEM images (secondary electron) of Pt/BMD electrodes deposited using (A) 10, (B) 25, and (C) 50 pulses, respectively. Pulse width 1 s. Current density  $0.50 \text{ mA}/\text{cm}^2$ .

deposition.<sup>39</sup> Increasing the number of pulses leads to an increase in the metal loading as more charge is passed; however, the nominal particle size increases and the particle coverage decreases. These trends are reflected in the Table I data. Depositing Pt with 10 pulses yields a nominal particle diameter of  $46 \pm 27 \text{ nm}$  [relative standard deviation (RSD) = 58%] and a nominal particle coverage of  $1.1 (\pm 0.6) \times 10^9 \text{ cm}^{-2}$ . Increasing the number of pulses to 25 ap-

**Table I. Particle analysis and hydrogen adsorption data for Pt-coated microcrystalline diamond films as a function of the pulse number.<sup>a</sup>**

No. of pulses	Mean particle size (nm)	Particle coverage (cm <sup>-2</sup> ) <sup>b</sup>	Hydrogen adsorption charge (mC/cm <sup>2</sup> ) <sup>b</sup>	RF
10	46 ± 27	1.1 (±0.6) × 10 <sup>9</sup>	0.066 ± 0.014	0.31
25	100 ± 85	9.8 (±4.4) × 10 <sup>8</sup>	0.13 ± 0.014	0.64
50	105 ± 66	3.8 (±0.1) × 10 <sup>8</sup>	0.21 ± 0.015	0.99

<sup>a</sup> Pulse width 1 s. Delay time 1 s. Current density 0.50 mA/cm<sup>2</sup> (geometric area). RF is the electrochemically active Pt area obtained from the hydrogen adsorption charge normalized to the geometric area of the diamond film (0.2 cm<sup>2</sup>).

<sup>b</sup> Values normalized to the geometric area of the diamond film.

proximately doubles the average particle diameter to 100 ± 85 nm (RSD = 85%) and halves the particle coverage to 9.8 (±4.4) × 10<sup>8</sup> cm<sup>-2</sup>. Increasing the number of pulses to 50 slightly increases the average particle diameter to 105 ± 66 nm (RSD = 63%) and further reduces the particle coverage to 3.8 (±0.1) × 10<sup>8</sup> cm<sup>-2</sup>. Careful examination of the images, in particular Fig. 1c, reveals that the particles are not smooth but rather are rough with a dendritic morphology.

Figure 2 shows background cyclic voltammetric i-E curves in 0.1 M HClO<sub>4</sub> for the Pt-coated microcrystalline thin-film electrodes formed with different pulse numbers. The scans were initiated at 200 mV with the forward sweep in the positive direction at a rate of 50 mV/s. All the voltammetric features characteristic of clean polycrystalline Pt are observed. The total current response increases with pulse number, which is consistent with an increase in the Pt loading. Even though the nominal particle diameter increases and the coverage decreases, the electrochemically active Pt increases.<sup>50</sup> The explanation for this is that the microscopic roughness of the deposits is increasing with pulse number, something that is evident in the SEM images (Fig. 1). The well-defined voltammetric signatures for Pt indicate that the metal particles are in good electrical communication with the current-collecting Si substrate through the boron-doped diamond film. The H<sup>+</sup> adsorption charge density, listed in Table I, was found by integrating the cathodic current for this reaction between 100 and -190 mV vs. Ag/AgCl and correcting for the double-

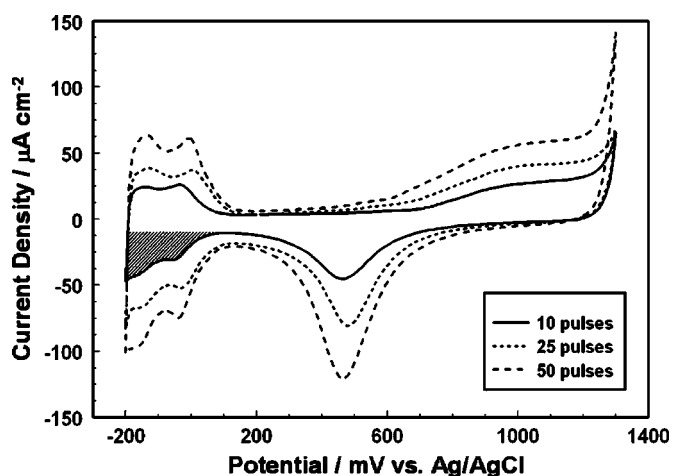


**Figure 2.** Cyclic voltammetric i-E curves in 0.1 M HClO<sub>4</sub> for Pt/BMD electrodes with Pt deposited using the different pulse numbers. Pulse width 1 s. Current density 0.50 mA/cm<sup>2</sup>. Scan rate 50 mV/s. The shaded region of the curve represents the charge associated with hydrogen adsorption. The current is normalized to the BMD geometric area, 0.2 cm<sup>2</sup>.

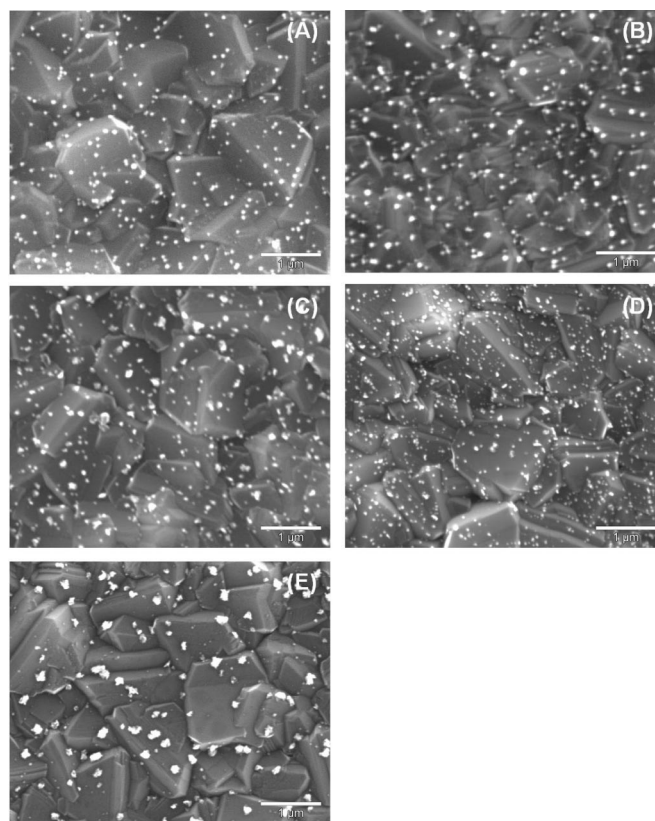


**Figure 3.** SEM images (secondary electron) of Pt/BMD electrodes deposited at pulse current densities of (A) 0.50, (B) 0.75, (C) 1.00, (D) 1.25, and (E), 1.50 mA/cm<sup>2</sup>, respectively. Pulse number 10. Pulse width 1 s. The scale bar in each image is 1 μm.

layer charging current (see the shaded region of the i-E curve in Fig. 2). The electrochemically active Pt areas were calculated to be 0.062, 0.13, and 0.20 cm<sup>2</sup>, respectively, for 10, 25, and 50 pulses (all electrodes possess the same deviation of ±0.016 cm<sup>2</sup>). Consequently, the roughness factor [RF, the electrochemically active Pt area/geometric area of the diamond electrode (0.2 cm<sup>2</sup>)] increases with pulse number, as is shown in Table I. It appears that the deposition of Pt on existing Pt clusters occurs more readily than on the bare diamond surface, and this creates a greater microscopic surface roughening with increasing pulse number. The loading increase was confirmed by AAS with calculated values of 2.4, 3.3, and 7.4 μg/cm<sup>2</sup> (measured for just one film at each pulse number) for 10, 25, and 50 pulses, respectively. An important performance parameter for electrocatalytic electrodes is the specific Pt surface area, defined as the electrochemically active Pt area normalized to the Pt loading. The specific surface areas were calculated to be 13, 20, and 14 m<sup>2</sup>/g Pt, respectively, for the three pulse numbers. Typical values for Pt electrocatalysts used in fuel cells are in the range of 100–200 m<sup>2</sup>/g Pt. Therefore, the specific surface areas on the planar diamond thin-film electrodes are about a factor of ten lower than what is desired for a fuel cell electrocatalyst.

The electrodeposition of Pt on microcrystalline diamond was also investigated as a function of the pulse current density from 0.50 to 1.50 mA/cm<sup>2</sup> (geometric area). The deposition was carried out using a pulse number of 10 and a pulse width of 1 s. Increasing the current density has the effect of increasing the activation overpotential (η). SEM images of metal-coated films are displayed in Fig. 3a-e. Table II presents a summary of the particle analysis data. Statistically, the nominal particle size is the same for all five current densities, ranging from 40 to 70 nm with an RSD of approximately 50%. The particle coverage increases from 1.3 (±1.0) to

**Table II. Particle analysis and hydrogen adsorption data for Pt-coated microcrystalline diamond films as a function of the pulse current density.<sup>a</sup>**

Pulse current density (mA/cm <sup>2</sup> ) <sup>b</sup>	Mean particle size (nm)	Particle coverage (cm <sup>-2</sup> ) <sup>b</sup>	Hydrogen adsorption charge (mC/cm <sup>2</sup> ) <sup>b</sup>
0.50	46 ± 27	1.1 (±0.6) × 10 <sup>9</sup>	0.066 ± 0.014
0.75	65 ± 37	1.5 (±0.4) × 10 <sup>9</sup>	0.095 ± 0.0069
1.00	59 ± 34	2.2 (±0.6) × 10 <sup>9</sup>	0.11 ± 0.0047
1.25	43 ± 27	7.5 (±0.9) × 10 <sup>9</sup>	0.16 ± 0.0051
1.50	68 ± 43	1.9 (±0.9) × 10 <sup>9</sup>	0.19 ± 0.031

<sup>a</sup> Pulse number 10. Pulse width 1 s. Delay time 1 s.

<sup>b</sup> Values normalized to the geometric area of the diamond film.

7.5 (±0.9) × 10<sup>9</sup> cm<sup>-2</sup> with current density up to 1.25 mA/cm<sup>2</sup>. For the highest current density, though, 1.50 mA/cm<sup>2</sup>, the particle coverage decreases to 1.9 (±0.9) × 10<sup>9</sup> cm<sup>-2</sup>. The film deposited at 1.25 mA/cm<sup>2</sup> has particles that are nominally the same size as those produced at 0.50 mA/cm<sup>2</sup>, but with a particle density nearly six times greater.

Figure 4 shows background cyclic voltammetric i-E curves for the Pt-coated microcrystalline thin-film electrodes formed with different pulse current densities in 0.1 M HClO<sub>4</sub>. The scans were initiated at 200 mV with the forward sweep in the positive direction at a rate of 50 mV/s. Again, all the voltammetric features characteristic of clean polycrystalline Pt are present. There is a progressive increase in the total voltammetric current as the deposition current density is increased from 0.50 to 1.50 mA/cm<sup>2</sup>, indicating the electrochemically active Pt area is increasing. The charge associated with the H<sup>+</sup> adsorption increases with deposition current density, as shown in Table II. This is due to an increase in the particle coverage, as is observed for the films coated at current densities from 0.50 to 1.25 mA/cm<sup>2</sup>, and the particle roughening.

Table III shows the estimated metal loading, the electrochemically active Pt area, the specific Pt area, and the roughness factor for the Pt-diamond electrodes formed at different pulse current densities. The electrochemically active Pt area and roughness factor both increase with deposition current density, as reflected in the voltammetric i-E curves. This is due to the increase in particle coverage (at least up to 1.25 mA/cm<sup>2</sup>) and microscopic roughness of the particles. The apparent metal loading increases from 2 to 6 μg Pt/cm<sup>2</sup>

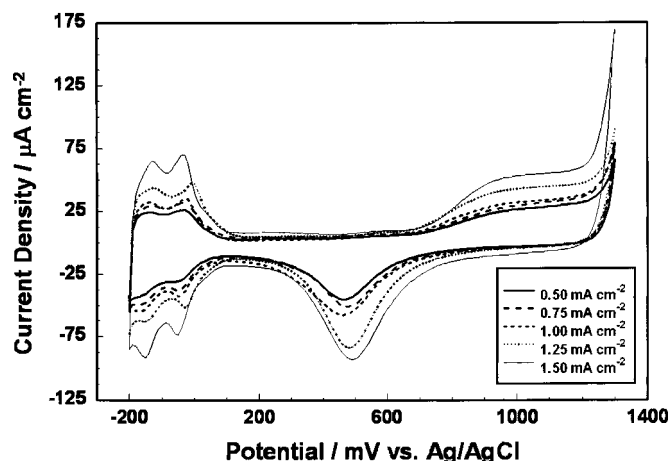


**Figure 4.** Cyclic voltammetric i-E curves in 0.1 M HClO<sub>4</sub> for Pt/BMD electrodes deposited with Pt at the different current densities. Pulse number 10. Pulse width 1 s. Scan rate 50 mV/s. The current is normalized to the BMD geometric area, 0.2 cm<sup>2</sup>.

**Table III. The electrochemically-active Pt area, specific Pt surface area, and roughness factor for Pt-coated diamond films deposited at different pulse current densities.<sup>a</sup>**

Pulse current density (mA/cm <sup>2</sup> ) <sup>b</sup>	Estimated loading (μg/cm <sup>2</sup> ) <sup>b</sup>	Electrochemically active Pt area (cm <sup>2</sup> )	Specific Pt surface area (m <sup>2</sup> /g Pt)	RF
0.50	2.4	0.062 ± 0.02	13	0.31
0.75	2.3	0.090 ± 0.007	20	0.45
1.00	2.2	0.11 ± 0.005	25	0.53
1.25	3.4	0.15 ± 0.004	22	0.74
1.50	4.3	0.18 ± 0.04	21	0.89

<sup>a</sup> Pulse number 10. Pulse width 1 s. Delay time 1 s. Loading estimated from AAS measurements of the dissolved metal deposits.

<sup>b</sup> Normalized to the geometric area of the diamond film.

with deposition current density. The specific Pt surface area ranges from 10 to 25 m<sup>2</sup>/g Pt with the values clustered around 20 m<sup>2</sup>/g Pt.

*Platinum deposition on nanocrystalline diamond.*—Pulsed galvanostatic deposition was also used to form Pt adlayers on boron-doped nanocrystalline diamond electrodes. Metal deposition is a surface “sensitive” charge-transfer process; therefore, the morphology and microstructure can strongly influence the nucleation mechanism. Comparing the deposition at these two diamond types provides insight about the influence of the film microstructure and morphology (e.g., grain boundaries, defects, facets, etc.) on the metal phase formation.

Two deposition conditions were evaluated, ten 1 s pulses at 0.50 and 1.25 mA/cm<sup>2</sup>. SEM images of these two metallized surfaces are shown in Fig. 5a (0.50 mA/cm<sup>2</sup>) and B (1.25 mA/cm<sup>2</sup>). Nanocrystalline diamond has a much smoother surface morphology than does microcrystalline diamond and a larger fraction of exposed grain boundary due to the smaller aggregate size.<sup>26,27</sup> It is also as corrosion resistant. The morphology consists of ca. 100 nm clusters of individual diamond crystallites that are 10–15 nm in diameter. We supposed that the higher fraction of grain boundary might lead to a higher nucleation site density for Pt and, in turn, to smaller particles with higher coverages. Other related work in our laboratory has demonstrated that this is in fact the case, as nanocrystalline outperforms microcrystalline diamond for the anodic stripping voltammetric determination of dissolved metal ions, in part, because metal phase formation on the former occurs with lower particle size and higher coverage.<sup>51</sup> The SEM images reveal metal deposits on the diamond surface, many of which appear to be located at the grain boundaries. Particle size analysis revealed a nominal diameter of 72 ± 41 nm (RSD = 57%), which is statistically similar to the particle size seen for microcrystalline diamond at the same current density. The particles are not as uniformly distributed over the surface as they are on the microcrystalline diamond surface, at least under these deposition conditions. The uneven distribution is reflected in a lower particle coverage of 6.1 (±4.6) × 10<sup>8</sup> cm<sup>-2</sup>, which is an order of magnitude less than that seen for the microcrystalline film.

The metal particles formed at 1.25 mA/cm<sup>2</sup> have a smaller nominal size of 25 ± 25 nm (RSD = 100%). The Pt particles are also more uniformly distributed over the surface and this is reflected in a larger particle coverage of 1.9 (±1.0) × 10<sup>10</sup> cm<sup>-2</sup>. Many of the metal particles appear to reside at the grain boundaries, which is consistent with these regions being the primary nucleation sites. This particle coverage is the highest observed for any of the diamond films under study, microcrystalline or nanocrystalline.

Figure 6 shows background cyclic voltammetric i-E curves in 0.1 M HClO<sub>4</sub> for Pt-coated nanocrystalline diamond thin-film electrodes deposited at 0.50 and 1.25 mA/cm<sup>2</sup>. The scans were initiated at 200 mV with the forward sweep in the positive direction at a rate

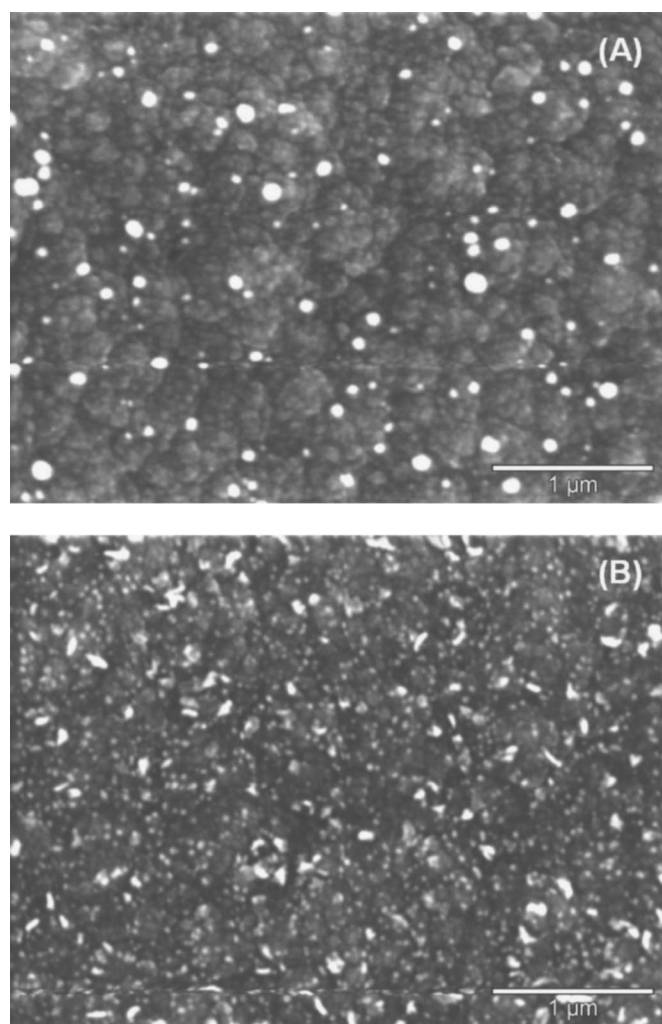


**Figure 5.** SEM images (secondary electron) of Pt/BND electrodes deposited at pulse current densities of (A) 0.50 and (B) 1.25 mA/cm<sup>2</sup>, respectively. Pulse number 10. Pulse width 1 s.

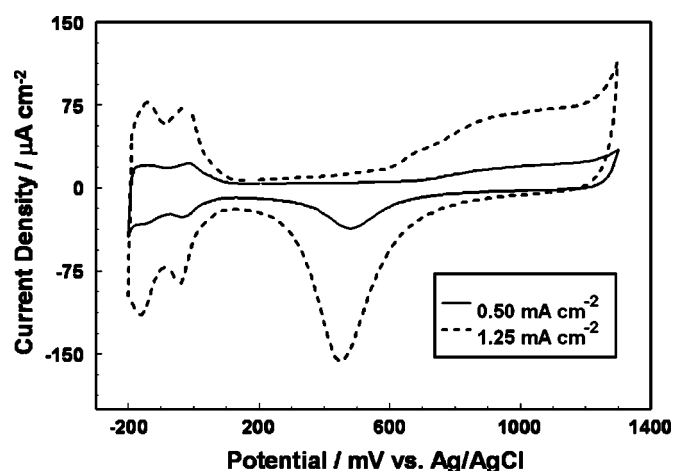


**Figure 6.** Cyclic voltammetric i-E curves in 0.1 M HClO<sub>4</sub> for Pt/BND electrodes deposited at 0.50 and 1.25 mA/cm<sup>2</sup>. Pulse number 10. Pulse width 1 s. Scan rate 50 mV/s. The current is normalized to the BND geometric area, 0.2 cm<sup>2</sup>.

of 50 mV/s. Again, all the voltammetric features characteristic of clean polycrystalline Pt are present. There is an increase in the total voltammetric current as the deposition current density is increased from 0.50 to 1.25 mA/cm<sup>2</sup>. This is consistent with the SEM data and results from an increased Pt loading and electrochemically active Pt area. It is worth noting that the nanocrystalline diamond electrode decorated with Pt at 1.25 mA/cm<sup>2</sup> shows much larger voltammetric currents than does the microcrystalline diamond electrode coated at the same current density. This is due to the smaller nominal particle size and larger particle coverage on the former. Interestingly, the i-E curve for the film coated at 1.25 mA/cm<sup>2</sup> exhibits a pre-peak prior to Pt oxide formation at ca. 700 mV. This pre-peak is associated with a Pt<sub>2</sub>OH species formed prior to the PtO monolayer in the plateau of the curve.<sup>52,53</sup> This peak may be due to Pt<sub>4</sub>OH formation on the (100)-oriented surfaces and/or Pt<sub>3</sub>OH formation on the (111)-oriented surfaces.<sup>53</sup>

The H<sup>+</sup> adsorption charge for the 0.50 and 1.25 mA/cm<sup>2</sup> films is 0.071 ± 0.010 and 0.25 ± 0.027 mC/cm<sup>2</sup>, respectively. The electrochemically active Pt area for the films is 0.068 ± 0.010 and 0.24 ± 0.031 cm<sup>2</sup>, respectively. These values result in roughness factors of 0.34 and 1.2. Calculations, based on AAS measurement data, revealed approximate Pt loadings of 1.4 and 2.4 μg/cm<sup>2</sup> for the 0.50 and 1.25 mA/cm<sup>2</sup> deposition currents, respectively. This translates into specific Pt surface areas of 24 and 50 m<sup>2</sup>/g Pt, respectively, which are the highest values we have recorded. It appears from these preliminary studies that the diamond film morphology and microstructure do indeed influence the nucleation and growth of Pt, and the highest specific areas are seen for the nanocrystalline films.

*Comparison studies with glassy carbon.*—In order to assess how metal deposition on diamond stacks up against deposition on sp<sup>2</sup> carbon electrodes, we conducted tests with glassy carbon. Based on the results discussed previously, the following conditions were selected for Pt deposition: Ten pulses of 1 s duration (delay time of 1 s between pulses) at 1.25 mA/cm<sup>2</sup>. SEM was used to evaluate the metal deposit. Particle size analysis revealed a particle diameter of 67 ± 55 nm (RSD = 82%) and a particle coverage of 5.3 (±1.3) × 10<sup>9</sup> cm<sup>-2</sup>. Cyclic voltammetry was employed to study the Pt activity for H<sup>+</sup> adsorption in 0.1 M HClO<sub>4</sub>. Integration of the i-E curves revealed an H<sup>+</sup> adsorption charge of 0.25 ± 0.018 mC/cm<sup>2</sup> (n = 3). This charge is similar to that seen for the nanocrystalline film and is a little larger than the value for microcrystalline diamond. The electrochemically active Pt area was calculated to be 0.24 ± 0.017 cm<sup>2</sup>. In summary, the metal phase formation on glassy carbon under these deposition conditions appears similar to what is seen for both diamond types in terms of the nominal particle size, coverage, and electrochemically active Pt area.

The specific Pt surface areas on diamond were in the range of 10-50 m<sup>2</sup>/g Pt (see Table III). These values are about a factor of 2-10 less than that for a typical electrocatalyst, 100-200 m<sup>2</sup>/g Pt. Gloaguen *et al.* reported values of 15-73 m<sup>2</sup>/g Pt for adlayers on three different types of carbon powders.<sup>54</sup> It is important to remember that the specific Pt surface area depends on the surface area of the carbon support. Kucernak *et al.* reported values of 20-50 m<sup>2</sup>/g Pt for electrodeposited adlayers on highly ordered pyrolytic graphite (HOPG).<sup>55</sup> Mo *et al.* reported on the immobilization of high-area Pt particles on glassy carbon with specific surface areas of ca. 30 m<sup>2</sup>/g Pt.<sup>56</sup> It is clear that the deposition on diamond yields electrocatalyst structures and activities that are similar to those for other sp<sup>2</sup> carbon support materials.

*Secondary diamond growth.*—The effect of a secondary diamond growth on the activity and stability of the Pt nanoparticles on microcrystalline diamond was investigated. A microcrystalline diamond thin-film electrode was coated with Pt using ten 1 s pulses duration at a current density of 1.25 mA/cm<sup>2</sup>. The initial H<sup>+</sup> adsorption charge in 0.1 M HClO<sub>4</sub> was 0.21 mC/cm<sup>2</sup>. This corresponds to an electrochemically active Pt area of 0.20 cm<sup>2</sup>. SEM images re-

vealed good metal coverage over the entire diamond surface. A nominal particle size of  $25 \pm 31$  nm and particle coverage of  $6.3 \times 10^9$  cm<sup>-2</sup> were determined from particle size analysis. No loss of Pt activity was observed after long-term solution exposure.

The metal-coated film was then subjected to a 30 min diamond deposition using a 0.5% CH<sub>4</sub>/H<sub>2</sub> source gas mixture at 1 kW, 200 sccm of total gas flow, 40 Torr, and ca. 800°C. These conditions are not necessarily optimum but rather were selected as a starting point. A nominal particle size of  $44 \pm 37$  nm and particle coverage of  $4.0 \times 10^9$  cm<sup>-2</sup> were determined from SEM images. The slightly larger nominal particle size and lower particle coverage are consistent with some coalescence of neighboring particles as the deposition temperature is ca. 800°C. More importantly, the particle shape changed from a rough, dendritic morphology to a smoother, more rounded morphology during the plasma treatment as a result of annealing effects.

After the secondary diamond growth, background cyclic voltammetric i-E curves were re-recorded in 0.1 M HClO<sub>4</sub>. The H<sup>+</sup> adsorption charge decreased to 0.015 mC/cm<sup>2</sup> (a factor of 10 loss), and this corresponds to a decreased electrochemically active Pt area of 0.014 cm<sup>2</sup>. There is clearly some loss in Pt activity due to particle coalescence and blockage by the diamond deposition. However, we suspect that a sizeable percentage of the loss seen here resulted not from "buried" particles but rather from poor alignment of the metallized electrode area inside the O-ring of the cell. The Pt exposed to the solution was anchored strongly and was extremely stable during an extended potential cycling period (1000 cycles) between -0.4 and 1.9 V vs. Ag/AgCl in 0.1 M HClO<sub>4</sub>. The maximum currents were near  $\pm 5$  mA/cm<sup>2</sup> at the two potential extremes. The H<sup>+</sup> adsorption charge actually increased slightly to 0.020 mC/cm<sup>2</sup> after cycling due to removal of carbon contaminants from the surface and particle roughening. In comparison, over 63% of the electrochemically active Pt was lost from a metal-coated diamond surface exposed to the same cycling conditions when no secondary diamond growth was applied. Research is ongoing to optimize the secondary diamond growth conditions in order to maximize the particle stability but minimize the extent of Pt activity loss.

### Discussion

The results presented herein demonstrate that pulsed galvanostatic deposition is a useful method for depositing nanometer-sized particles of Pt on diamond electrode surfaces. In terms of the nominal particle size, particle coverage, and electrochemically active Pt, pulsed deposition is superior to constant current deposition.<sup>19-21</sup> The optimum conditions for depositing Pt on both types of diamond were ten 1 s pulses at 1.25 mA/cm<sup>2</sup> with a 1 s delay between each pulse. The nominal particle size of ca. 25 nm and particle coverage of ca.  $10^{10}$  cm<sup>-2</sup> seen for the nanocrystalline film are good values for a supported electrocatalyst. These values are also comparable to what was achieved with glassy carbon, indicating that metal deposition on diamond occurs in a similar manner to that on an sp<sup>2</sup> carbon electrode.

The basic objective of pulsed deposition is to reduce the average growth rate of particles, which is expected to reduce the interactions between closely spaced ones. While we did not comprehensively investigate the nucleation and growth mechanism, there are some trends in the data that shed light on the mechanistic aspects of the deposition. The nominal particle size increases and the particle coverage decreases with increasing pulse number at a fixed deposition current density (*i.e.*, constant  $\eta$ ). It appears from our results that the initial nucleation occurs at a fixed number of sites and that new Pt particles nucleate and grow on existing Pt rather than forming at new sites on the diamond surface. This explains the rough, dendritic morphology of the deposits. With longer pulse times and therefore more charge passed, the growth of neighboring nuclei becomes coupled after a sufficient growth time. This results in particle coalescence, a reduced particle coverage, and an increased nominal particle size.

Increasing the deposition current density (*i.e.*, increasing  $\eta$ ) pro-

duces an increased particle coverage up to the 1.25 mA/cm<sup>2</sup> level, at which point particle coalescence begins to occur. This trend appears more consistent with nucleation via a progressive mechanism. Growth of new Pt particles appears to occur on both existing Pt sites and at sites on the diamond surface. We have previously found, using EC-AFM and i-t transients, that the nucleation of Cu on microcrystalline diamond follows an instantaneous mechanism at low overpotentials ( $\eta < 500$  mV) and shifts to a progressive mechanism at higher overpotentials.<sup>57</sup> Vinokur *et al.* studied the electrodeposition of Ag and Hg on diamond using i-t transients and found that the mechanism of nucleation depended on the overpotential and the metal ion concentration.<sup>52</sup> At low overpotentials, instantaneous nucleation was observed and at high overpotentials or metal ion concentrations the process became progressive. Preliminary results using EC-AFM and i-t transients have revealed that the electrodeposition of the more electronegative Zn on microcrystalline diamond follows a more progressive nucleation mechanism at both low and high overpotentials.<sup>57</sup>

Finally, it is useful to consider what challenges there are to electrochemically producing a dimensionally uniform metal adlayer on polycrystalline diamond. The physical aspects of the deposition method certainly will impact the dimensional uniformity of the metal deposits, as does the heterogeneity of the electrode's microstructural and electronic properties. Electrically conducting diamond is a quite heterogeneous electrode material, both microstructurally and electronically. The polycrystalline films possess diamond crystallites or grains, grain boundaries, and a multitude of other defects (*e.g.*, dislocations, step edges, etc.). The microcrystalline films are rough with valleys between the crystallites that could serve as higher coordination sites for metal phase formation, whereas the nanocrystalline films are smooth but possess a high fraction of exposed grain boundary due to the small crystallite size. We suppose that the grain boundaries are the primary nucleation sites initially and, therefore, the high grain boundary density leads to a smaller nominal particle size and larger particle coverage.

The electronic properties of diamond also play a key role on the dispersion and uniformity of metal adlayers. The electronic properties of diamond are controlled in a complex manner by (i) the boron doping level and distribution throughout the film,<sup>58-63</sup> (ii) incorporated hydrogen which can act both as an acceptor and provide a charge carrier or as a donor and passivate a boron acceptor,<sup>64-68</sup> and (iii) defect density.<sup>63,69,70</sup> Of these, the boron doping level and distribution are probably the most influential. Furthermore, it is known that boron incorporates into polycrystalline diamond with different concentrations depending on the growth sector.<sup>71,72</sup> The boron concentration in the {111} growth sector is five or more times greater than that found in the {100} sector. In other words, polycrystalline diamond, particularly the microcrystalline films, is composed of sites of faster (reversible) kinetics where the dopant level is high and sites of slower kinetics (less reversible) where there is less dopant. We have recently observed such electrical and electrochemical heterogeneity using CP-AFM mapping and scanning electrochemical microscopy (SECM) of microcrystalline diamond films.<sup>73</sup> Similar heterogeneity is seen for the nanocrystalline films as well. An example of this is shown in Fig. 7a-d. Both height mode images and conductivity maps are presented over a  $10 \times 10$  (A) and  $1 \times 1$   $\mu\text{m}$  (C) area. Nodular features are seen in the images with a size of 100-500 nm. These nodular features are actually clusters of diamond grains that are 10-15 nm in diameter.<sup>26,27</sup> The intersection of the clusters constitute the grain boundaries. The figure also shows conductivity maps over the same areas (B and D). In these measurements, a Au-coated Si tip contacting the surface was rastered over an area and the current was measured using a bias voltage of +2 V ( $E_{\text{tip}} - E_{\text{substrate}}$ ). The bright areas correspond to regions of higher conductivity and the darker features to regions of lower conductivity. Clearly, there are conductivity variations across the surface. The more conductive regions do not appear to be exclusively at the grain boundaries. The higher resolution image in Fig. 7d reveals that the distance between the conducting regions is on the order of 200

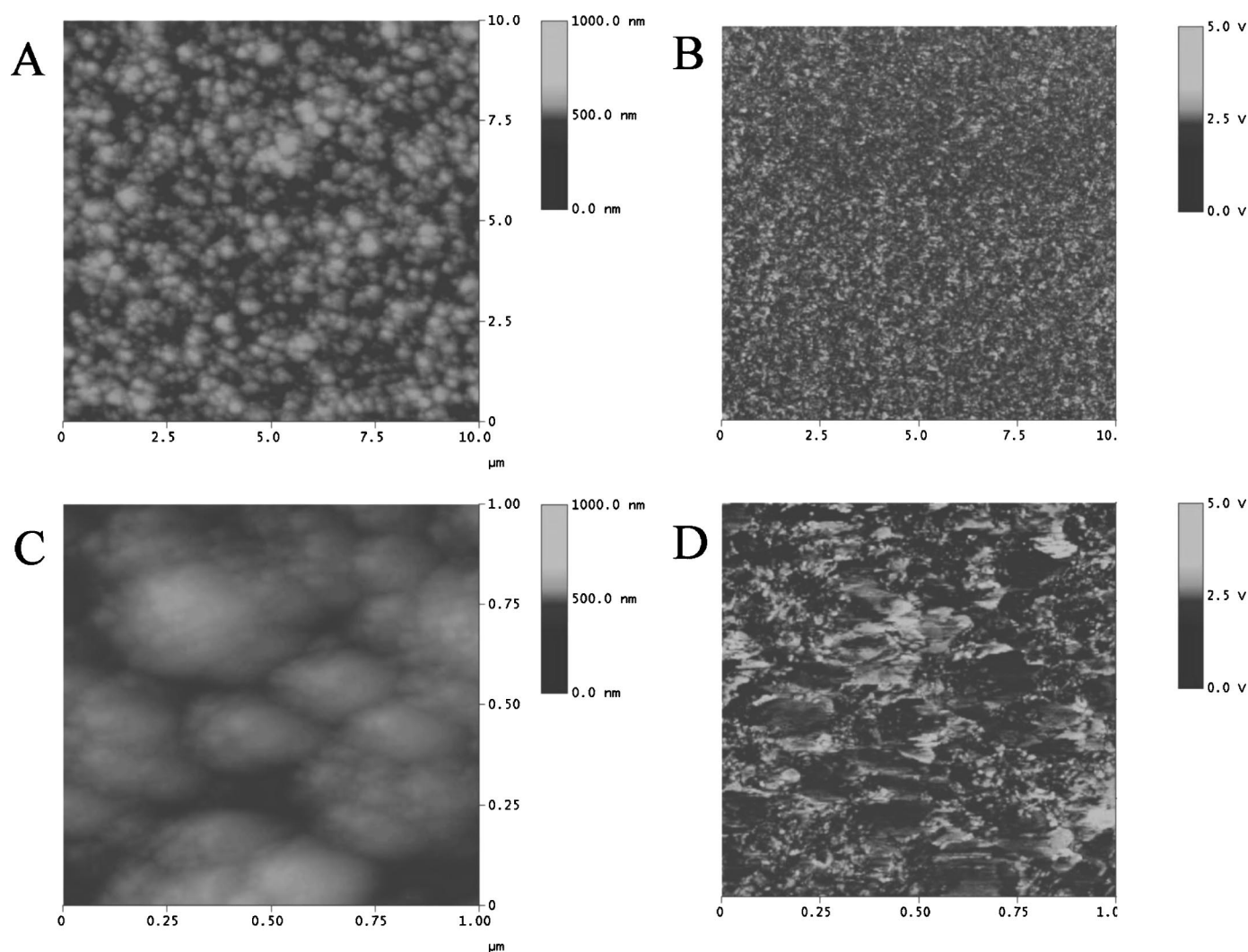


**Figure 7.** AFM height mode images (air) of a boron-doped nanocrystalline diamond thin film over (A) a  $10 \times 10$  and (C) a  $1 \times 1$   $\mu\text{m}$  area. Simultaneously recorded conductivity maps of the same regions (B and D) with a bias voltage of +2 V ( $E_{\text{tip}} - E_{\text{substrate}}$ ).

-300 nm in some cases. These data are important and have implications for the dimensional uniformity of the metal adlayers. The take-home message is that inherently there is going to be spatial variations in the metal adlayer formation due to this heterogeneity in electrical conductivity. It remains to be proven but it is logical to suppose that the conductive regions are the sites where initial nucleation occurs. Therefore, the fraction of these conductive sites on a film will control the initial nucleation density. A similar conclusion was recently reached by Enea *et al.* in their AFM study of the electrodeposition of Pt on polycrystalline diamond.<sup>33</sup>

### Conclusions

The pulsed galvanostatic deposition of Pt electrocatalyst particles on boron-doped microcrystalline and nanocrystalline diamond thin film was investigated. The deposition was studied as a function of the pulse number and current density, while maintaining a pulse length of 1 s and a duty cycle of 50%. Pulsed galvanostatic deposition produced a nominal particle size that is an order of magnitude smaller than that previously observed for constant current deposition.<sup>19,20</sup> Deposition using ten pulses and a current density of  $1.25 \text{ mA/cm}^2$  yielded the most active electrocatalyst on both diamond types, in terms of the nominal particle size, particle coverage, and the highest specific Pt surface area. For both electrode types, the nominal particle size was *ca.* 30 nm with an RSD of 50% or less, and the particle coverage was *ca.*  $10^7$  to  $10^{10} \text{ cm}^{-2}$  under the opti-

um deposition conditions. The typical specific surface areas were in the  $10\text{-}50 \text{ m}^2/\text{g}$  Pt range. The deposition of Pt on diamond compared favorably to deposition on glassy carbon. The microstructure and morphology of diamond were observed to strongly influence the nucleation and growth of Pt. The highest specific surface area of  $50 \text{ m}^2/\text{g}$  Pt was observed for the nanocrystalline film, which possesses a high fraction of exposed grain boundaries. The grain boundaries appear to serve as the primary nucleation sites on this film. Finally, the influence of the film's electronic properties on the metal phase formation was investigated. The polycrystalline diamond film is quite heterogeneous in terms of the electrical conductivity, as evidenced by CP-AFM. The film is composed of sites of faster (reversible) kinetics where the dopant level is high and sites of slower kinetics (less reversible) where there is less dopant. It is supposed that the regions of high electrical conductivity serve as the initial nucleation sites.

### Acknowledgments

This work was sponsored by the U.S. Department of Energy, Office of Science (DE-FG03-95ER14577), and the Center for Fundamental Materials Research at Michigan State University.

*Michigan State University assisted in meeting the publication costs of this article.*

## References

1. E. Antolini, *J. Mater. Sci.*, **38**, 2995 (2003).
2. F. Rodriguez-Reinoso, *Carbon*, **36**, 159 (1998).
3. L. Carrette, K. A. Friedrich, and U. Stimming, *Fuel Cells*, **1**, 5 (2001).
4. J. Y. Lucisano, J. C. Armour, and D. A. Gough, *Anal. Chem.*, **59**, 736 (1987).
5. A. Damjanovic and V. Brusic, *Electrochim. Acta*, **12**, 615 (1967).
6. N. Giordano, E. Passalacqua, L. Pino, A. S. Aricó, V. Antonucci, M. Vivaldi, and K. Kinoshita, *Electrochim. Acta*, **36**, 1979 (1991).
7. N. M. Markovic, T. J. Schmidt, V. Stamenkovic, and P. N. Ross, *Fuel Cells*, **1**, 105 (2001).
8. H.-H. Yang and R. L. McCreery, *J. Electrochem. Soc.*, **147**, 3420 (2000).
9. T. Yano, E. Popa, D. A. Tryk, K. Hashimoto, and A. Fujishima, *J. Electrochem. Soc.*, **146**, 1081 (1999).
10. E. Yeager, *Electrochim. Acta*, **29**, 1527 (1984).
11. I. Morcos and E. Yeager, *Electrochim. Acta*, **15**, 953 (1970).
12. E. Yeager, J. A. Molla, and S. Gupta, in *Electrochemistry of Carbon*, S. Sarangapani, J. R. Akridge, and B. Schumm, Editors, PV 84-5, p. 123, The Electrochemical Society Proceedings Series, Pennington, NJ (1984).
13. E. Yeager and D. Tryk, in *Proceedings of the 33rd International Power Sources Symposium*, Cherry Hill, NJ, June 13-16, 1988, The Electrochemical Society, Inc. (1988).
14. B. C. H. Steele and A. Heinzl, *Nature (London)*, **414**, 345 (2001).
15. E. Auer, A. Freund, J. Pietsch, and T. Tacke, *Appl. Catal., A*, **173**, 259 (1998).
16. A. J. Appleby, *Corrosion (Houston)*, **43**, 398 (1987).
17. R. Makharia, P. Yu, J. Pisco, S. Kocha, and H. Gasteiger, Paper 1888 presented at The Electrochemical Society Meeting, Honolulu, HI, Oct 3-8, 2004.
18. J. Wang, G. M. Swain, T. Tachibana, and K. Kobashi, *Electrochem. Solid-State Lett.*, **3**, 286 (2000).
19. J. Wang and G. M. Swain, *Electrochem. Solid-State Lett.*, **5**, E4 (2002).
20. J. Wang and G. M. Swain, *J. Electrochem. Soc.*, **150**, E24 (2003).
21. M. Hupert, A. Muck, J. Wang, J. Stotter, Z. Cvackova, S. Haymond, Y. Show, and G. M. Swain, *Diamond Relat. Mater.*, **12**, 1940 (2003).
22. G. M. Swain, *J. Electrochem. Soc.*, **141**, 3382 (1994).
23. J. Xu, M. C. Granger, Q. Chen, J. W. Strojek, T. E. Lister, and G. M. Swain, *Anal. Chem.*, **69**, 591A (1997).
24. M. C. Granger, J. Xu, J. W. Strojek, and G. M. Swain, *Anal. Chim. Acta*, **397**, 145 (1999).
25. G. M. Swain, A. B. Anderson, and J. C. Angus, *MRS Bull.*, **23**, 56 (1998).
26. Q. Chen, D. M. Gruen, A. R. Krauss, T. D. Corrigan, M. Witek, and G. M. Swain, *J. Electrochem. Soc.*, **148**, E44 (2001).
27. Y. Show, M. A. Witek, P. Sonthalia, and G. M. Swain, *Chem. Mater.*, **15**, 879 (2003).
28. A. E. Fischer, Y. Show, and G. M. Swain, *Anal. Chem.*, **76**, 2553 (2004).
29. M. Awada, J. W. Strojek, and G. M. Swain, *J. Electrochem. Soc.*, **142**, L42 (1995).
30. Y. Zhang, S. Asahina, S. Yoshihara, and T. Shirakashi, *Electrochim. Acta*, **48**, 741 (2003).
31. S. Nakabayashi, D. A. Tryk, A. Fujishima, and N. Ohta, *Chem. Phys. Lett.*, **300**, 409 (1999).
32. N. Vinokur, B. Miller, Y. Avyigal, and R. Kalish, *J. Electrochem. Soc.*, **146**, 125 (1999).
33. O. Enea, B. Riedo, and G. Dietler, *Nano Lett.*, **2**, 241 (2002).
34. E. Budevski, G. Staikov, and W. J. Lorenz, in *Electrochemical Phase Formation and Growth*, VCH, New York (1996).
35. M.-S. Löffler, B. Groß, H. Natter, R. Hempelmann, T. Krajewski, and J. Divisek, *Phys. Chem. Chem. Phys.*, **3**, 333 (2001).
36. J. V. Zoval, R. M. Stiger, P. R. Biernacki, and R. M. Penner, *J. Phys. Chem.*, **100**, 837 (1996).
37. J. V. Zoval, J. Lee, S. Gorer, and R. M. Penner, *J. Phys. Chem. B*, **102**, 1166 (1998).
38. J. L. Fransaer and R. M. Penner, *J. Phys. Chem. B*, **103**, 7643 (1999).
39. S. Gorer, H. Liu, R. M. Stiger, M. P. Zach, J. V. Zoval, and R. M. Penner, in *Metal Nanoparticles*, D. L. Feldheim and C. A. Foss, Jr., Editors, p. 237, Marcel Dekker, Inc. New York (2002).
40. R. M. Penner, *J. Phys. Chem. B*, **105**, 8672 (2001).
41. R. M. Penner, *J. Phys. Chem. B*, **106**, 3339 (2002).
42. H. Liu, F. Favier, K. Ng, M. P. Zach, and R. M. Penner, *Electrochim. Acta*, **47**, 671 (2001).
43. H. Liu and R. M. Penner, *J. Phys. Chem. B*, **104**, 9131 (2000).
44. G. Gunawardena, G. Hills, I. Montenegro, and B. Scharifker, *J. Electroanal. Chem. Interfacial Electrochem.*, **138**, 225 (1982).
45. P. Allongue and E. Souteyrand, *J. Electroanal. Chem. Interfacial Electrochem.*, **286**, 217 (1990).
46. M. C. Granger, M. Witek, J. Xu, J. Wang, M. Hupert, A. Hanks, M. D. Koppang, J. E. Butler, G. Lucazeau, M. Mermoux, J. W. Strojek, and G. M. Swain, *Anal. Chem.*, **72**, 3793 (2000).
47. S. Ranganathan, T.-C. Kuo, and R. L. McCreery, *Anal. Chem.*, **71**, 3574 (1999).
48. J. Perez, A. A. Tanaka, E. R. Gonzalez, and E. A. Ticianelli, *J. Electrochem. Soc.*, **141**, 431 (1994).
49. J. M. D. Rodríguez, J. A. H. Melián, and J. P. Peña, *J. Chem. Educ.*, **77**, 1195 (2000).
50. A. Essalik, K. Amouzegar, and O. Savadogo, *J. Appl. Electrochem.*, **25**, 404 (1995).
51. P. Sonthalia, E. McGaw, Y. Show, and G. M. Swain, *Anal. Chim. Acta*, **522**, 35 (2004).
52. H. Angerstein-Kozłowska, B. E. Conway, and W. B. A. Sharp, *J. Electroanal. Chem. Interfacial Electrochem.*, **43**, 9 (1973).
53. B. V. Tilak, B. E. Conway, and H. Angerstein-Kozłowska, *J. Electroanal. Chem. Interfacial Electrochem.*, **48**, 1 (1973).
54. F. Gloaguen, J.-M. Leger, and C. Lamy, *J. Appl. Electrochem.*, **27**, 1052 (1997).
55. A. R. Kucernak, P. B. Chowdhury, C. P. Wilde, G. H. Kelsall, Y. Y. Zhu, and D. E. Williams, *Electrochim. Acta*, **45**, 4483 (2000).
56. Y. Mo, S. Sarangapani, A. Le, and D. A. Scherson, *J. Electroanal. Chem.*, **528**, 35 (2002).
57. J. Wang, Ph.D. Dissertation, Michigan State University, East Lansing, MI (2002).
58. J. T. Huang, C. S. Hu, J. Hwang, H. Chang, and L. J. Lee, *Appl. Phys. Lett.*, **67**, 2382 (1995).
59. K. Nishimura, K. Das, and J. T. Glass, *J. Appl. Phys.*, **69**, 3142 (1991).
60. N. Vinokur, B. Miller, Y. Avyigal, and R. Kalish, *J. Electrochem. Soc.*, **143**, L238 (1996).
61. M. N. Latto, G. Pastor-Moreno, and D. J. Riley, *Electroanalysis*, **16**, 434 (2004).
62. R. F. Mamin and T. Inushima, *Phys. Rev. B*, **63**, 033201 (2001).
63. W. Zhu, in *Diamond: Electronic Properties and Applications*, L. S. Pan and D. R. Kania, Editors, Chap. 5, Kluwer Academic Publishers, Boston, MA (1995).
64. M. I. Landstrass and K. V. Ravi, *Appl. Phys. Lett.*, **55**, 1391 (1989).
65. K. Hayashi, S. Yamanaka, H. Okushi, and K. Kajimura, *Appl. Phys. Lett.*, **68**, 376 (1996).
66. H. J. Looi, R. B. Jackman, and J. S. Foord, *Appl. Phys. Lett.*, **72**, 353 (1998).
67. H. J. Looi, L. Y. S. Pang, A. B. Molloy, F. Jones, J. S. Foord, and R. B. Jackman, *Diamond Relat. Mater.*, **7**, 550 (1998).
68. H. J. Looi, M. D. Whitfield, J. S. Foord, and R. B. Jackman, *Thin Solid Films*, **343-344**, 623 (1999).
69. B. Fiegl, R. Kuhnert, M. Ben-Chorin, and F. Koch, *Appl. Phys. Lett.*, **65**, 371 (1994).
70. D. Stenbach, A. Flöter, H. Güttler, R. Zachai, and P. Ziemann, *Diamond Relat. Mater.*, **8**, 273 (1999).
71. T. Kolber, K. Piplits, R. Haubner, and H. Hutter, *Fresenius' J. Anal. Chem.*, **365**, 636 (1999).
72. K. Ushizawa, K. Watanabe, T. Ando, I. Sakaguchi, M. Nishitani-Gamo, Y. Sato, and H. Kanada, *Diamond Relat. Mater.*, **7**, 1719 (1998).
73. K. B. Holt, A. J. Bard, Y. Show, and G. M. Swain, *J. Phys. Chem. B*, **108**, 15117 (2004).